International Journal of Applied Power Engineering (IJAPE)
Vol. 14, No. 4, December 2025, pp. 769~782
ISSN: 2252-8792, DOI: 10.11591/ijape.v14.i4.pp769-782

Performance enhancement using sensor and sensorless control techniques for a modified bridgeless Ćuk converter-based BLDC motor in EV applications

W. Margaret Amutha, S. Premalatha, M. Karthikeyan
Department of Electrical and Electronics Engineering, SRM Institute of Science and Technology, Ramapuram Campus, Chennai, India

Article Info

Article history:

Received Oct 7, 2024
Revised Jul 5, 2025
Accepted Aug 3, 2025

Keywords:

Back EMF
BLDC motor
Electric vehicle
Modified bridgeless Ćuk converter
Solar PV source
Speed controller

ABSTRACT

This work proposes a solar photovoltaic (PV)-powered, modified bridgeless Ćuk converter tailored for electric vehicle applications. It overcomes limitations such as high ripple, reduced power density, significant switching losses, and complex circuit structures in traditional designs. The system integrates a boost converter with a bridgeless Ćuk topology to ensure a reliable and efficient direct current (DC) power output. Performance evaluation includes sensor-based and sensorless speed control techniques—pulse width modulation (PWM), proportional integral derivative (PID), back electromotive force (EMF), and spider controllers—under both no-load and full-load scenarios. Key parameters such as rise time, overshoot, settling time, and steady-state error are analyzed. MATLAB/Simulink simulations indicate that the spider controller delivers superior dynamic behavior and stability. A 48 W, 1500 rpm hardware prototype confirms the simulation outcomes, demonstrating the practical viability and effectiveness of the proposed converter.

Corresponding Author:

M. Karthikeyan
Department of Electrical and Electronics Engineering
SRM Institute of Science and Technology, Ramapuram Campus
Ramapuram, Chennai, Tamil Nadu, India
Email: karthikm14@srmist.edu.in

1. INTRODUCTION

Adoption of renewable energy in electric vehicles (EVs) has increased, with solar photovoltaic (PV) systems favored for their clean and reliable power [1]. Standard maximum power point tracking (MPPT) methods like perturb and observe (P&O) and incremental conductance (IC) are generally used but struggle under fast-changing conditions [2]. To improve performance, adaptive variants such as dynamic P&O [3] and modified IC [4] have been proposed. Metaheuristic approaches like particle swarm optimization (PSO) [5], genetic algorithm (GA) [6], and ant colony optimization (ACO) [7] offer better accuracy but are computationally heavy. Hybrid methods, including PSO-P&O [8], enhance tracking speed and stability. Recently, AI-based techniques using machine learning and fuzzy logic have shown strong adaptability to variable irradiance [9], [10]. This paper proposes an AI-assisted P&O method to boost MPPT efficiency in solar-powered EVs. DC-DC converters such as Luo, buck-boost, zeta, sepic, and Ćuk have been explored extensively for EV applications [11]-[13], but traditional converters often suffer from limited voltage gain and high switching losses. To overcome these limitations, this work integrates a modified bridgeless Ćuk converter with a conventional boost converter, improving voltage gain, efficiency, and reducing switching stress.

For propulsion, brushless direct current (BLDC) motors are preferred in EVs for their high efficiency, low noise, durability, and strong speed–torque characteristics, making them suitable for heavy-

duty applications [14]. To enhance motor performance, both sensorless and algorithm-based control methods are used. Sensorless techniques, such as those by Real *et al.* [15] and Awchar *et al.* [16], estimate rotor position using back electromotive force (EMF), eliminating physical sensors [17]. Digital control methods based on Newton's law also offer simple, effective solutions [18]. Intelligent controllers like GA-tuned fuzzy logic and queen bee evolution algorithms aim to improve dynamic response, though some show limitations in transient performance [19]-[24]. Optimization methods, including DE, PSO, spider, and population-based algorithms, have demonstrated improvements in reducing rise time, overshoot, and settling time [25]-[28].

Traditional controllers like pulse width modulation (PWM), back EMF, integral derivative (PID), and hysteresis band are commonly used for BLDC motor speed control [29]-[31]. While PWM and back EMF offer precise regulation, they often introduce ripple current and torque instability. PID controllers, especially when algorithmically tuned, provide stable and accurate control. Spider-based controllers have recently drawn significant interest for their enhanced dynamic response. However, existing literature [32]-[35] often examines these controllers in isolation, lacking direct comparisons with other methods. This study addresses that gap by performing a comparative analysis of PWM, PID, back EMF, and spider controllers using MATLAB/Simulink. The evaluation focuses on key performance indicators such as maximum overshoot, settling time, and steady-state error. The paper is organized as: Sections 1 and 2 provide the introduction and describe the BLDC motor model along with the proposed modified bridgeless Ćuk converter. Section 3 outlines the different speed control strategies employed. Section 4 presents the analysis of both transient and steady-state responses. Section 5 details the simulation outcomes, and section 6 ends up with summarized findings and suggested future research directions.

2. SYSTEM CONFIGURATION OVERVIEW

Figure 1(a) illustrates the full EV system, while Figure 1(b) highlights the BLDC motor control used to compare speed control methods. The setup includes a solar PV source, battery, modified bridgeless DC-DC converter, three-phase inverter, BLDC motor, and controller. Solar PV serves as the main power source, with the battery ensuring stability during fluctuations. The converter adjusts PV voltage to meet motor demands, and excess energy charges the battery. The inverter supplies AC to the motor, while the controller regulates speed based on error signals. BLDC motors are preferred in EVs for their efficiency and low maintenance. Speed control is implemented using sensor-based and sensorless methods. MATLAB/Simulink is used for system modeling and performance analysis.

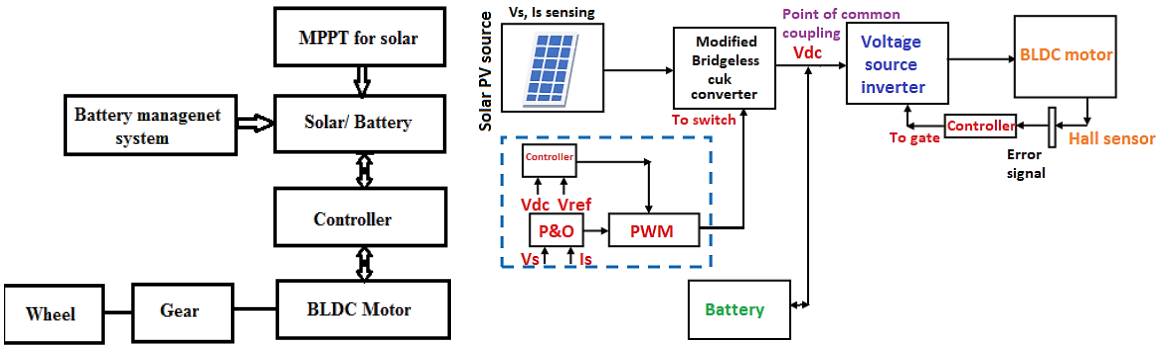

Figure 1. Schematic structure of EV: (a) EV structure and (b) schematic of a BLDC motor with a controller

3. COMPUTATIONAL MODEL OF THE SYSTEM

Figure 2 depicts the layout of a BLDC motor drive control system developed for electric vehicle applications. This configuration comprises five components: voltage source, buck converter, battery source, inverter, and the BLDC motor. Outlined below is the modeling process of each system.

3.1. Analytical model of BLDCM

BLDCM used in this work operates in three phases, as it gives low torque and better efficiency. Some assumptions are made to build the analytical model of BLDCM. The stator winding is equally spaced with 60º. The BLDC motor modeling is written by considering V_{as}, V_{bs}, V_{cs} as stator voltages, stator resistance as R, i_a, i_b, i_c as stator currents, and back EMF voltages as E_a, E_b, and E_c. For the design of a BLDC motor, we will neglect armature reaction, magnetic saturation, hysteresis, and vortex losses.

$$\begin{bmatrix} V_{as} \\ V_{bs} \\ V_{cs} \end{bmatrix} = \begin{bmatrix} R & 0 & 0 \\ 0 & R & 0 \\ 0 & 0 & R \end{bmatrix} * \begin{bmatrix} i_a \\ i_b \\ i_c \end{bmatrix} + \begin{bmatrix} L-M & 0 & 0 \\ 0 & L-M & 0 \\ 0 & 0 & L-M \end{bmatrix} * \frac{d}{dt} \begin{bmatrix} i_a \\ i_b \\ i_c \end{bmatrix} + \begin{bmatrix} E_a \\ E_b \\ E_c \end{bmatrix} \quad (1)$$

$$ia + ib + ic = 0 \quad (2)$$

The line voltages are:

$$\begin{bmatrix} V_{ab} \\ V_{bc} \\ V_{ca} \end{bmatrix} = * \begin{bmatrix} i_a \\ i_b \\ i_c \end{bmatrix} + \begin{bmatrix} L-M & 0 & 0 \\ 0 & L-M & 0 \\ 0 & 0 & L-M \end{bmatrix} * \frac{d}{dt} \begin{bmatrix} i_a \\ i_b \\ i_c \end{bmatrix} + \begin{bmatrix} E_a - E_b \\ E_b - E_c \\ E_c - E_a \end{bmatrix} \quad (3)$$

where L is phase winding inductance (Henry) and M is mutual inductance (Henry). So, the torque (T) is expressed as (4).

$$T = \frac{1}{\omega} (E_a i_a + E_b i_b + E_c i_c) \quad (4)$$

The nominal voltage and current of 35 V, 5 A, with the 2500 rpm rated speed rate is considered for simulation. Hence, BLDC motor's transfer function is as (5).

$$G(s) = \frac{0.01}{0.05S^2 + 0.6S + 0.1} \quad (5)$$

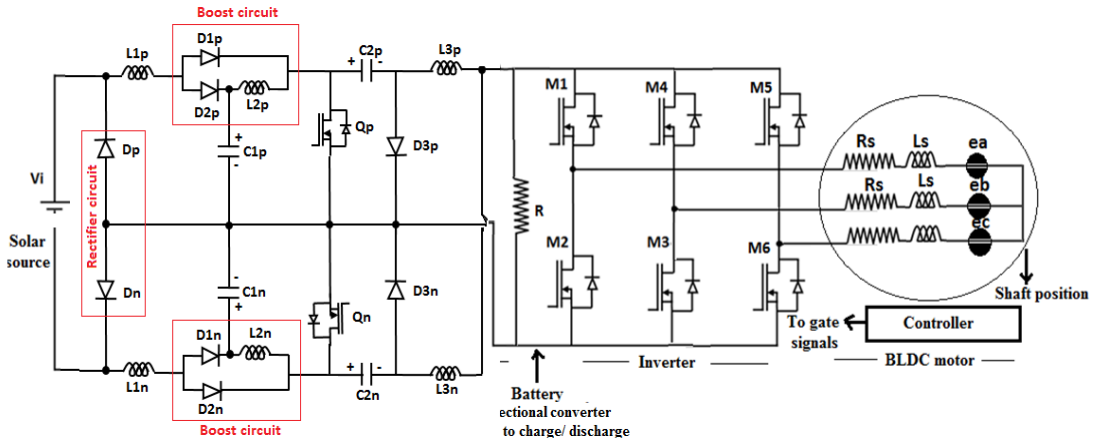

Figure 2. Configuration of a BLDC motor with a speed control drive

3.2. System elements

3.2.1. Solar PV (SPV) system

A single diode circuit is employed in constructing the SPV cell. The mathematical model of a PV cell is implemented using the MATLAB/Simulink platform. Figure 3(a) shows a PV topology construction.

An AI-based P&O MPPT algorithm is used to track the maximum power point of the solar PV source. The corresponding MATLAB code is provided. The I-V characteristics of the PV module are shown in Figure 3(b). Figure 4(a) displays the gate pulse generated by the MPPT algorithm, which drives the modified Ćuk converter. For simulation, solar insolation is set at 230 V, 6.5 A, 1.5 kW, and 900 W/m². Output voltage, current, and power from the solar source are shown in Figure 4(b).

a. Modified Ćuk converter and three-phase inverter

The mathematical model of the system is formulated as follows. The modified Ćuk converter model is given as (6).

$$E_{dc-out}(t) = E_{dc-in}(t) * \eta_{dc} \quad (6)$$

Table 1 outlines the different operating modes of the modified Ćuk converter. The DC output from the solar system is first converted to AC, which serves as the converter's input, comprising both positive and negative half-cycles. Based on these cycles, the converter operates in two switching modes defined by the ON/OFF states of its switches. Figures 5(a) to 5(d) illustrate the functioning of each mode.

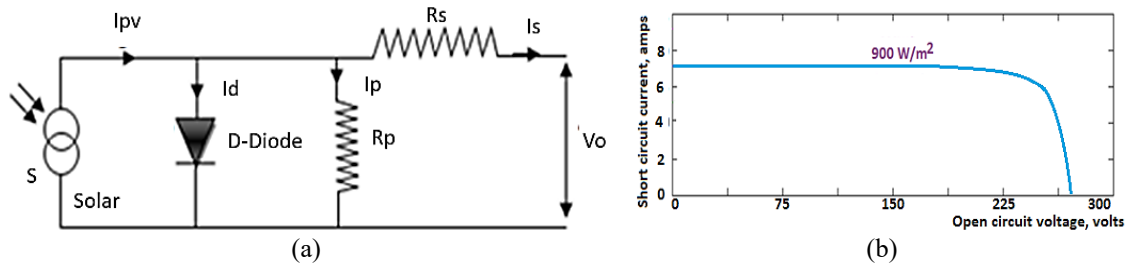

(a) (b)

Figure 3. The SPV cell: (a) PV cell and (b) IV characteristics of a solar source

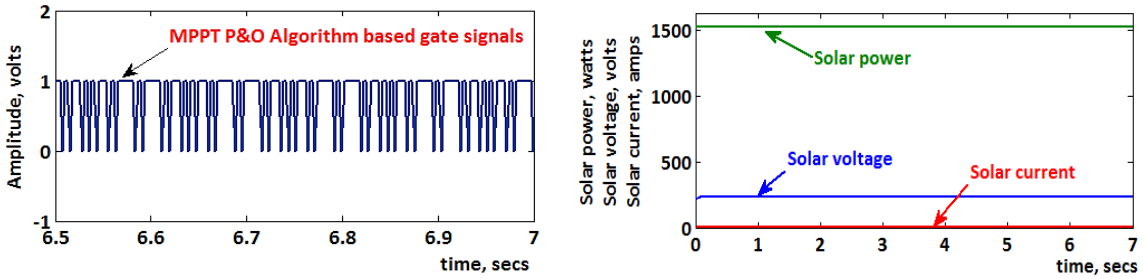

(a) (b)

Figure 4. Gate pulses: (a) gate pulses from MPPT and (b) voltage, current and power output of the solar

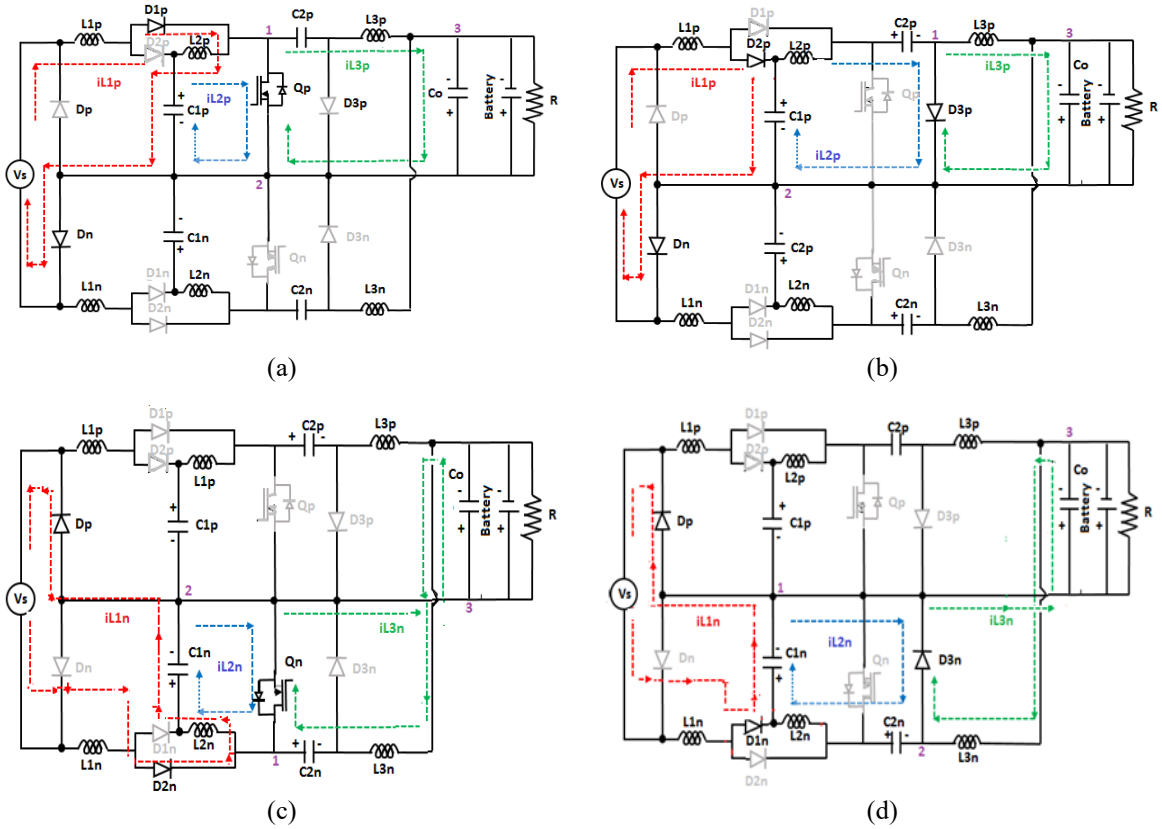

Figure 5. Modes of operation: (a) Mode 1: Qp- ON, Qn- OFF, (b) Mode 2: both Qp, Qn- OFF (positive input cycle), (c) Mode 3: Qp- OFF, Qn- ON, and (d) Mode 4: both Qp and Qn- OFF (negative input cycle)

Table 1. Functional operation of converter

Modes	Active lines	Working
1	Qp-ON Qn-OFF	In the positive half-cycle of the input voltage, diodes D_P and D_{1P} become forward biased. Inductors L_{1P} and L_{2P} charge capacitor C_{1P}, while L_{3P} transfers energy to capacitor C_{2P}. At the same time, the output capacitor C_O supplies power to the load, and any surplus energy is directed to the battery for storage.
2	Qp-OFF Qn-OFF	In the positive half-cycle of the input signal, diodes D_n and D_{1P} conduct, enabling inductors L_{1P} and L_{2P} to store energy and charge capacitor C_{1P}. The stored energy in C_{1P} is then transferred to capacitor C_{2P}. Meanwhile, inductor L_{3P} delivers energy to the output capacitor C_O, which powers the connected load. When the wind system fails to generate sufficient energy, the battery steps in to supply the additional required power.
3	Qp-OFF Qn-ON	In the negative half-cycle, diodes DP and D2n conduct, allowing inductors L_{1n} and L_{2n} to charge capacitor C_{1n}. This capacitor energizes inductor L_{2n}, while L3n and capacitor C_{2n} supply power to output capacitor C_O, which drives the load. When wind energy is insufficient, the battery provides backup power; any surplus energy is stored for later use.
4	Qp-OFF Qn-OFF	In the negative half-cycle, diodes D_P, D_{2n}, and D_{3n} are forward biased. Inductors L_{1P} and L_{2P} charge capacitor C_{1P}, while energy from C_{1n} is transferred to C_{2n}. Inductor L_{3n} powers the output capacitor C_O, which supplies the load. When wind energy is insufficient, the battery meets the excess power demand.

The design parameters of the converter are determined from the analytical model. Converter specifications are calculated using (7) and (8).

Let $L_{1_P} = L_{1_n}$, $L_{2_P} = L_{2_n}$ and $C_{1_P} = C_{1_n}$,$C_{2_P} = C_{2_n}$

$$L_1 = \frac{V_S * d_1}{\Delta I_{L_1} * F_s} = 1\ mH \text{ and } L_2 = L_3 = \frac{V_S * d_2}{2 * \Delta I_{L_2} * F_s} = 100\ \mu H \quad (7)$$

$$C_1 = C_2 = \frac{I_O * d_1}{\Delta V_{C_1} * F_S} = 0.8\ \mu F \text{ and } C_O = \frac{P_O}{4 * \pi * \Delta V_{C_O} * F_S * V_O} = 440\ \mu F \quad (8)$$

The volt-second balance method is utilized for inductors L_1 and L_2, as calculated in (9) and (10).

$$V_{C_1} * \left(\frac{1}{2 * L_1}\right) - V_S * \left(\frac{1}{L_1}\right) = 0 \quad (9)$$

$$V_{C_2} * d_1 = V_{C_0} \text{ or } V_{C_2} = \frac{V_{C_0}}{d_1} \quad (10)$$

From the derived equations, V_{C_0} is obtained as shown in (11).

$$V_{C_0} = -V_S * \frac{(2 - d_1) * d_1}{(1 - d_1)} \quad (11)$$

The charge balance approach is applied to C_1, C_2, and C_O for steady-state analysis, as presented in (12)-(14).

$$I_{L_1} * \left(\frac{-1}{C_1}\right) + I_{L_2} * \left(\frac{-1}{C_1}\right) = 0 \quad (12)$$

$$I_{L_2} * \left(\frac{1}{C_2}\right) + I_{L_3} * \left(\frac{1 - d_1}{C_2}\right) = 0 \quad (13)$$

$$I_{L_3} * \left(\frac{1}{C_O}\right) + I_{L_3} * \left(\frac{1}{C_O}\right) - V_{C_0} * \left(\frac{1}{R * C_O}\right) = 0 \quad (14)$$

Solving the equations gives the relation as (15).

$$I_O = \frac{V_{C_0}}{R} = I_{L_1} * \frac{1}{(1 - d_1)} + I_{L_2} * \frac{1}{(1 - d_2)} \quad (15)$$

Edc-out(t) is the DC link energy output in kWh, while Edc-in(t) is the input voltage converted to AC by the converter, with ηdc as its efficiency. Figure 6 shows the output voltage, current, and power of the modified Ćuk converter. Surplus energy charges the battery, and the DC output is later converted to AC.

b. Battery

The solar source relies on storage element to balance the fluctuations on load demand and the power generated. A battery of 48 V, 16 Ah has been chosen. Figure 7 illustrates battery voltage, current, and SOC. The charging/ discharging capacity of the battery can be calculated as:

$$E_{Battery}(t) = Battery\ Capacity\ (Ah) / Battery\ Current\ (A) \quad (16)$$

$$E_{Battery}(t) = E_{Battery}(t-1) - E_{Needed}(t) \quad (17)$$

$$\text{DOD (Depth of discharge)} = (1 - d) * 100 \quad (18)$$

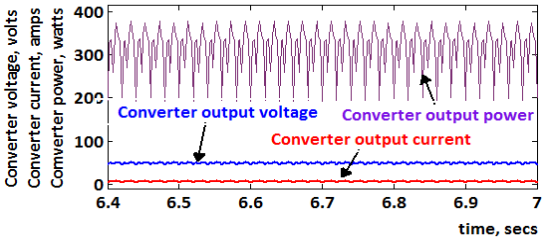

Figure 6. Converter output voltage, current, and power

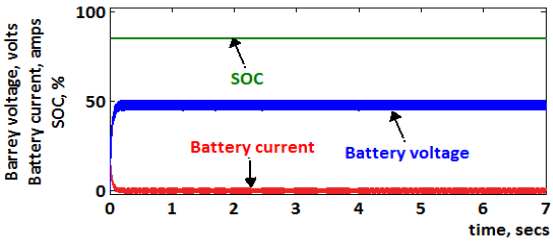

Figure 7. Battery voltage, current, and SOC

3.3. Approaches to BLDC motor speed regulation

This work applies three techniques to control BLDC motor speed. The actual speed is compared with a reference, and the resulting error signal generates gate pulses to achieve the target speed.

3.3.1. PWM speed control technique

Figure 8(a) shows the commonly used speed control setup. The speed error is fed to a PWM generator, which adjusts the duty cycle to maintain the target speed. Figure 8(b) displays the inverter's PWM pulses.

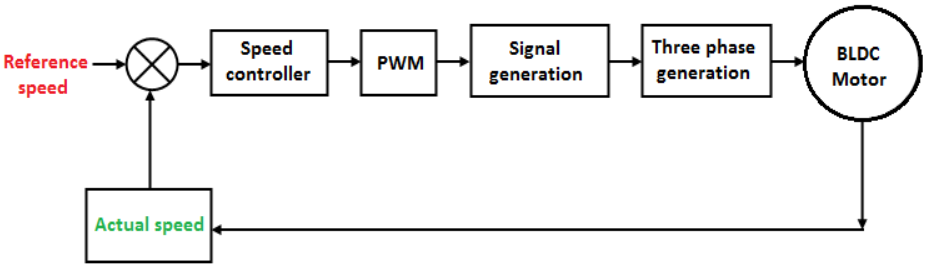

(a)

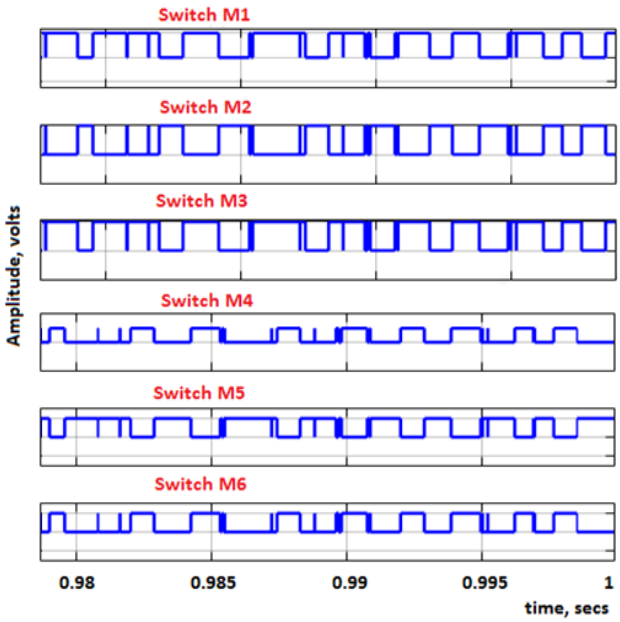

(b)

Figure 8. PWM generation: (a) block diagram of PWM generator and (b) PWM pulses

3.3.2. PID based speed control strategy

The pictorial diagram of a PID speed control technique is given in Figure 9(a). It consists of the actual process, PID controller, and a feedback system. In the absence of disturbances, it is assumed that the controlled variable c(t)c(t)c(t) closely approximates the desired input r(t). Gating pulses obtained using PID controller is shown in Figure 9(b). The transfer function is expressed as (19).

$$G_c(s) = K_P + \frac{K_i}{S} + K_d\, s \tag{19}$$

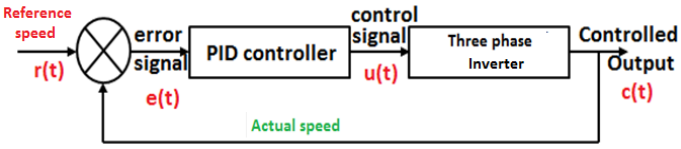

(a)

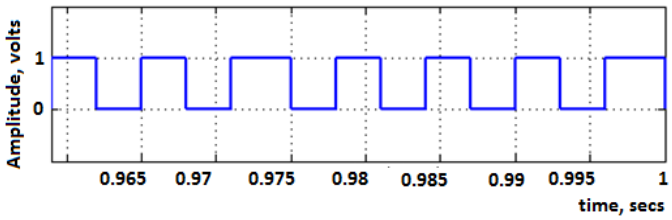

(b)

Figure 9. PID controller: (a) representation of PID controller and (b) gating pulses from PID controller

3.3.3. Back EMF (sensor less technique)

In this method, switches are triggered by digital pulses from the back EMF observer. These pulses are decoded into gating signals. Inverter commutation is performed every 60 degrees to maximize torque output, aligning the rectangular current with the back EMF. Figure 10(a) presents the back EMF observer, while Figure 10(b) displays the corresponding gating signals.

$$E_b = K_e * \omega_e \text{ and } \omega_e = \frac{\omega_{mech}}{P_n} \tag{20}$$

Where ω_{mech} is the angular velocity, ω_e is the rotor speed, and P_n is the pole pair.

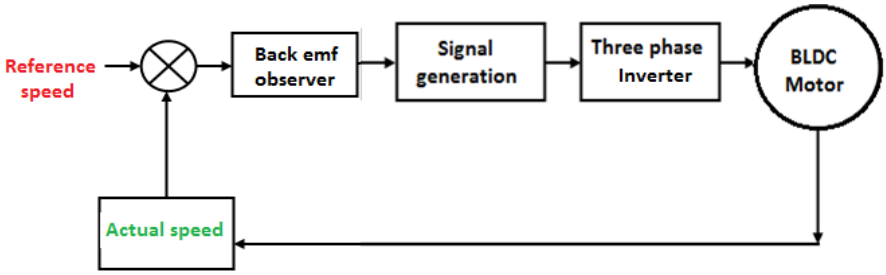

(a)

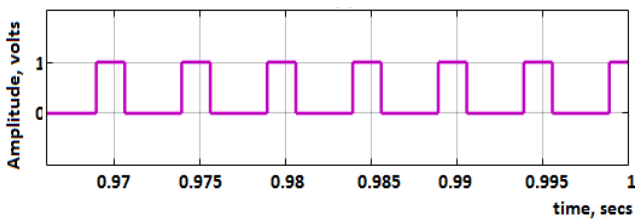

(b)

Figure 10. Back EMF observer: (a) functional representation and (b) gating through back EMF observer

3.3.4. Spider control method

The spider-based controller generates switching sequences by comparing the reference signal with feedback. Gate pulses are derived using speed and Hall sensor outputs. Back EMF and rectified voltage are compared to produce signals. The method is named for its resemblance to a spider's web-building process.

The switching follows the pattern shown in Table 2. The estimated Hall position is given in Table 3. The controlled gate pulses applied to the three-phase inverter are given in Figure 11(a). The estimated Hall position wave form is given in Figure 11(b).

Table 2. Switching sequence of spider controller

EMF_a	EMF_b	EMF_c	Q1	Q2	Q3	Q4	Q5	Q6
-1	1	0	0	0	1	1	0	0
1	-1	0	1	0	0	0	0	1
-1	0	1	0	1	0	1	0	0
1	0	-1	1	0	0	0	1	0
0	-1	-1	0	1	0	0	0	1
0	1	-1	0	0	1	0	1	0

Table 3. Estimated hall position

h_a	h_b	h_c	EMF_a	EMF_b	EMF_c
0	0	0	-1	1	0
0	0	1	1	-1	0
0	1	0	-1	0	1
0	1	1	1	0	-1
1	0	0	0	-1	-1
1	0	1	0	1	-1
1	1	0	0	1	-1
1	1	1	0	0	0

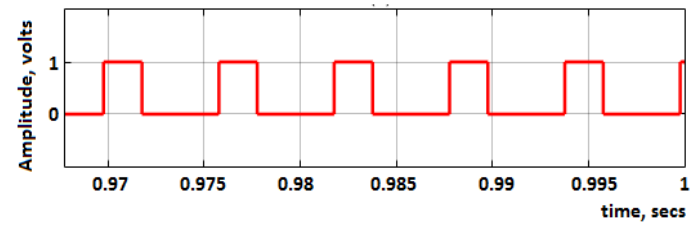

(a)

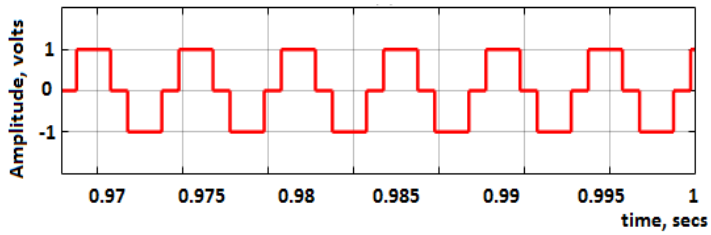

(b)

Figure 11. Spider controller: (a) duty cycle for inverter and (b) estimated Hall position waveform

4. RESULTS AND DISCUSSION

The proposed topology and control strategy are simulated in MATLAB/Simulink using the BLDC motor model derived from (1)–(8), with motor and converter specifications listed in Tables 4 and 5. BLDC motor speed is controlled using PWM, PID, back EMF, and spider controllers. A 3-arm inverter supports PWM at 500 Hz. Figure 12(a) shows a 1.32 overshoot with 0.03 s settling time. Figure 12(b) and Table 6 compare all controllers at 2500 rpm under no-load and full-load.

Table 4. Specifications of BLDC motor

Parameter	Rating
Phase	3
Number of pole	4 pairs- 8 poles
Square flange size	80 mm
Voltage rating	170 V
Rating of the current	18 A
Rating of the power	3 kW
Speed rating	2500 rpm
Holding torque	2.4 Nm
Peak torque	6.6 Nm
DC voltage	35 V

Table 5. Simulation specifications of converter

Parameter	Rating
Load voltage	48 V
Load power	230 W
Load current	6.5 A
Inductor L_1	1476 µH
Inductors $L_2 = L_3$	1450 µH
Capacitors $C_1 = C_2$	0.8 µF
Capacitor C_O	440 µF
Switching frequency (Fs)	50 kHz
Resistive load, R_L	7.38 Ω

In this work, component values are kept constant across all controller types. Table 7 shows that the PWM controller results in higher peak overshoot, while the spider controller achieves better performance in terms of overshoot (Mp), rise time (tr), and settling time (ts), along with strong starting torque. Figure 13(a) displays stable stator current with the spider controller under varying loads. Figure 13(b) shows consistent electromagnetic torque (Te) at both no-load and full-load, indicating low torque ripple. Figure 13(c) confirms smooth operation with stable, sinusoidal back EMF. Figures 14(a) and 14(b) illustrate steady DC output voltage and current. Table 8 compares no-load output current, highlighting the spider controller's superior stability and efficiency.

Table 6. Comparison of different controllers

Controller types	Dynamic response			Static response
	Rise time, tr	Settling time, ts	Peak overshoot, Mp	Steady state error, ess
PWM	0.05 s-(NL)	0.25 s- (NL)	43%- (NL)	0.8- (NL)
	0.02 s-(FL)	0.22s- (FL)	45%- (FL)	0.8- (FL)
PID	0.05 s-(NL)	0.12 s- (NL)	38%- (NL)	0.8- (NL)
	0.019s-(FL)	0.2 s- (FL)	41%- (FL)	0.8- (FL)
Back EMF	0.04 s-(NL)	0.15 s- (NL)	13%- (NL)	0.8- (NL)
	0.02 s-(FL)	0.2 s- (FL)	11%- (FL)	0.8- (FL)
Spider	1e-6 s-(NL)	2e-6 s- (NL)	1%- (NL)	1e-3- (NL)
	1e-6 s-(FL)	2e-6 s- (FL)	0.01%- (FL)	1e-3- (FL)

Table 7. Parameter of PID controller

Parameter	Values
Proportional (Kp)	19.2
Integral (Ki)	2.002
Derivative (Kd)	0.00001

Table 8. Load current RMS comparison using various controllers

Method	PWM	PID	EMFG	Spider
Output current RMS at load no load	0.6646	0.97	0.52	0.4046
Applicable	Difficult	moderate	easy	Very easy

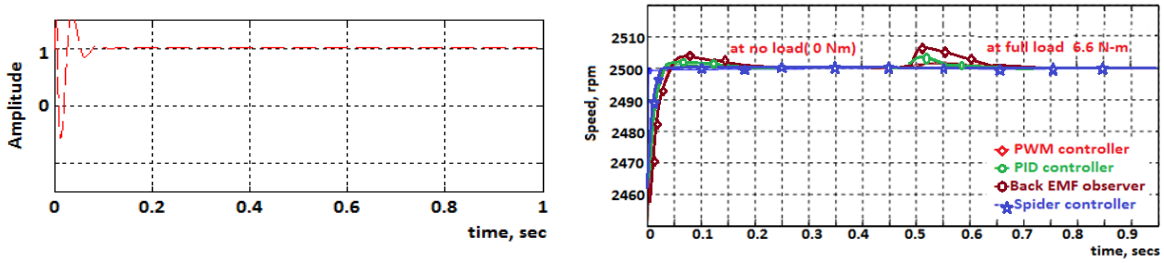

(a) (b)

Figure 12. Responses under various conditions: (a) step response and (b) speed controller (at various load)

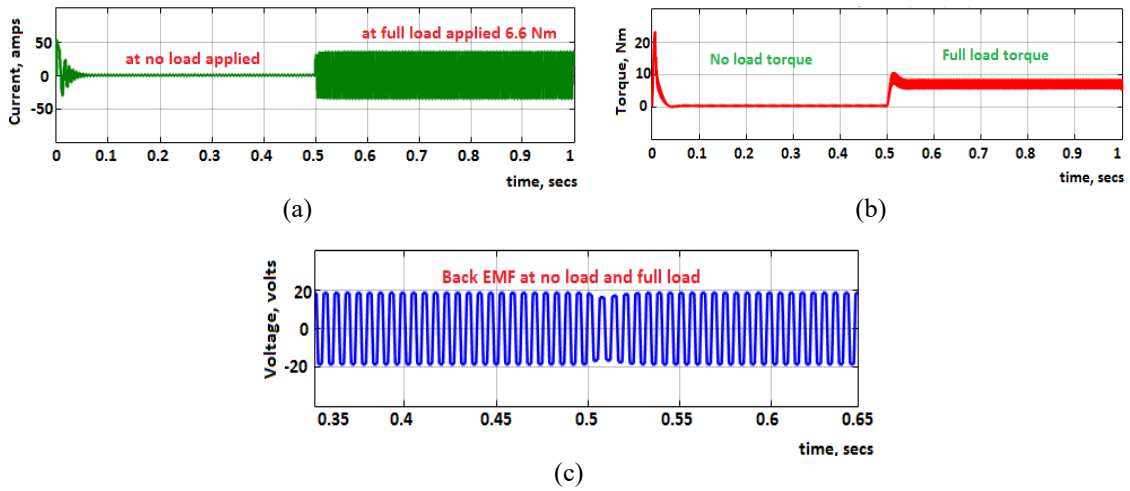

(a) (b)

(c)

Figure 13. Output of controllers: (a) stator current, (b) electromagnetic torque, and (c) back EMF

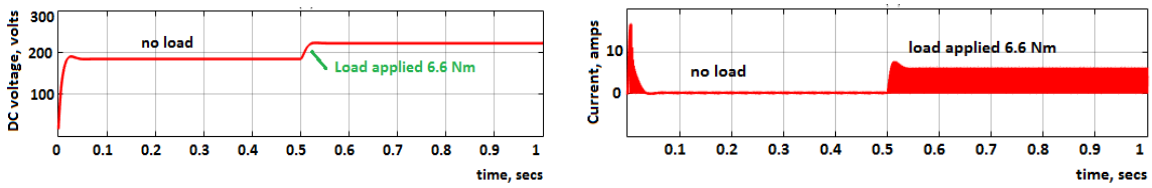

(a) (b)

Figure 14. Output of converter: (a) DC load voltage and (b) DC load current

4.1. Hardware implementation

Figure 15(a) shows BLDC motor speed control using a spider controller, while Figure 15(b) compares spider and PWM controllers. The spider controller demonstrates better transient and steady-state performance with fewer oscillations and more stable response. In contrast, the PWM controller responds slower and shows more fluctuations under load changes. A 24 V, 2 A, 48 W, and 1500 rpm BLDC motor is used. Current is measured using the cost-effective ACS712 sensor, and the HW IR201 sensor detects motor variations. A Hall Effect sensor monitors magnetic fields. Output voltage and current are fed into a PIC18F2550 controller powered by 5 V. This reprogrammable, flexible PIC interfaces with Simulink, enabling closed-loop control through PC connection.

The components used for implementing hardware are given in Table 9. PWM signals obtained from the PIC controller that is applied to the inverter is given in Figure 16(a). It displayed a properly modulated PWM signal from the PIC controller, which, when applied to the inverter, results in a controlled and efficient motor operation. Figures 16(b) and 16(c) display the back EMF and stator current respectively. From Figures 16(b) and 16(c), it is inferred that the minimized harmonic distortion ensures smoother motor operation and enhances the overall efficiency of the system. Any deviations from the sinusoidal shape, such as spikes or ripples, indicate problems with the inverter's switching pattern or mechanical issues like load fluctuations.

Figures 17(a) and 17(b) show the measured DC load voltage and current as 25V and 2A. The voltage across inductor L3p and output capacitor Co is 24.9 V and 1.3 V, as shown in Figures 17(c) and 17(d). Hardware waveforms of input voltage and current are presented in Figures 17(e) and 17(f). Figures 18(a) and 18(b) display the gate signals for Qp and Qn.

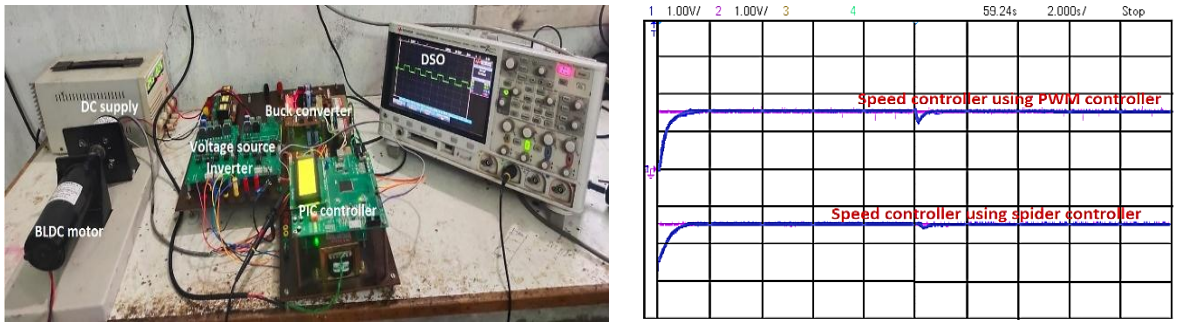

(a) (b)

Figure 15. Hardware results: (a) BLDC motor with spider controller and (b) speed controller using PWM/spider

Table 9. Rating of hardware components

Specifications	Rating
Input AC voltage	24 V
Source power	72 W
Source current	3 A
Load voltage	24 V
Load power	48 W
Load current	2 A
Inductor L_1	1476 µH
Inductors $L_2 = L_3$	1450 µH
Capacitors $C_1 = C_2$	0.8 µF
Capacitor C_O	440 µF
Lamp load R_L	12 Ω

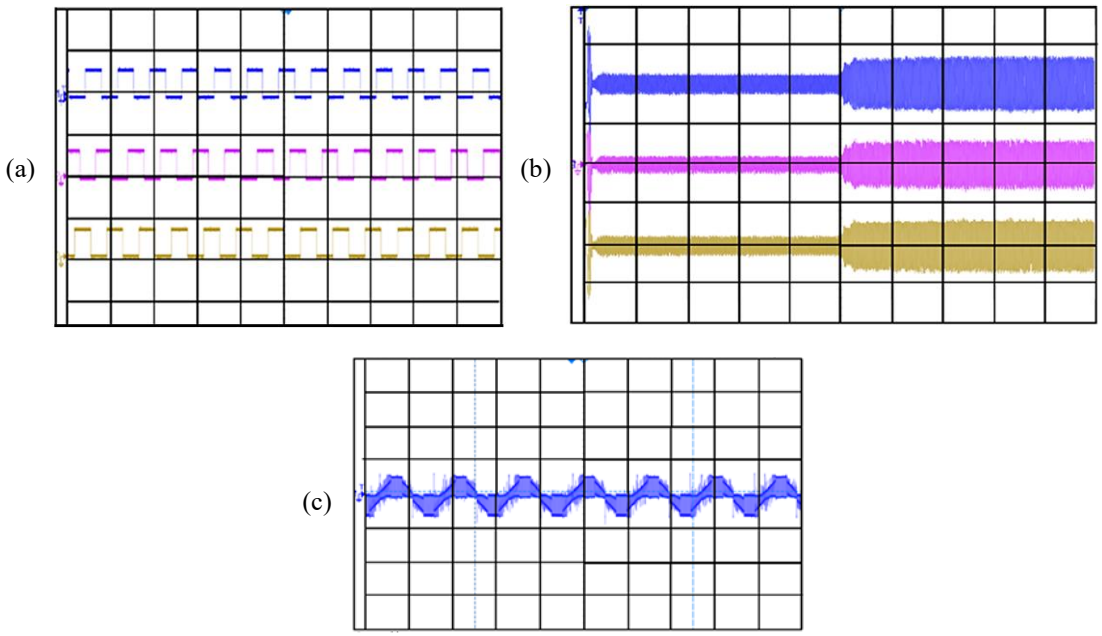

Figure 16. Hardware outputs: (a) PWM signals, (b) stator current, and (c) back EMF

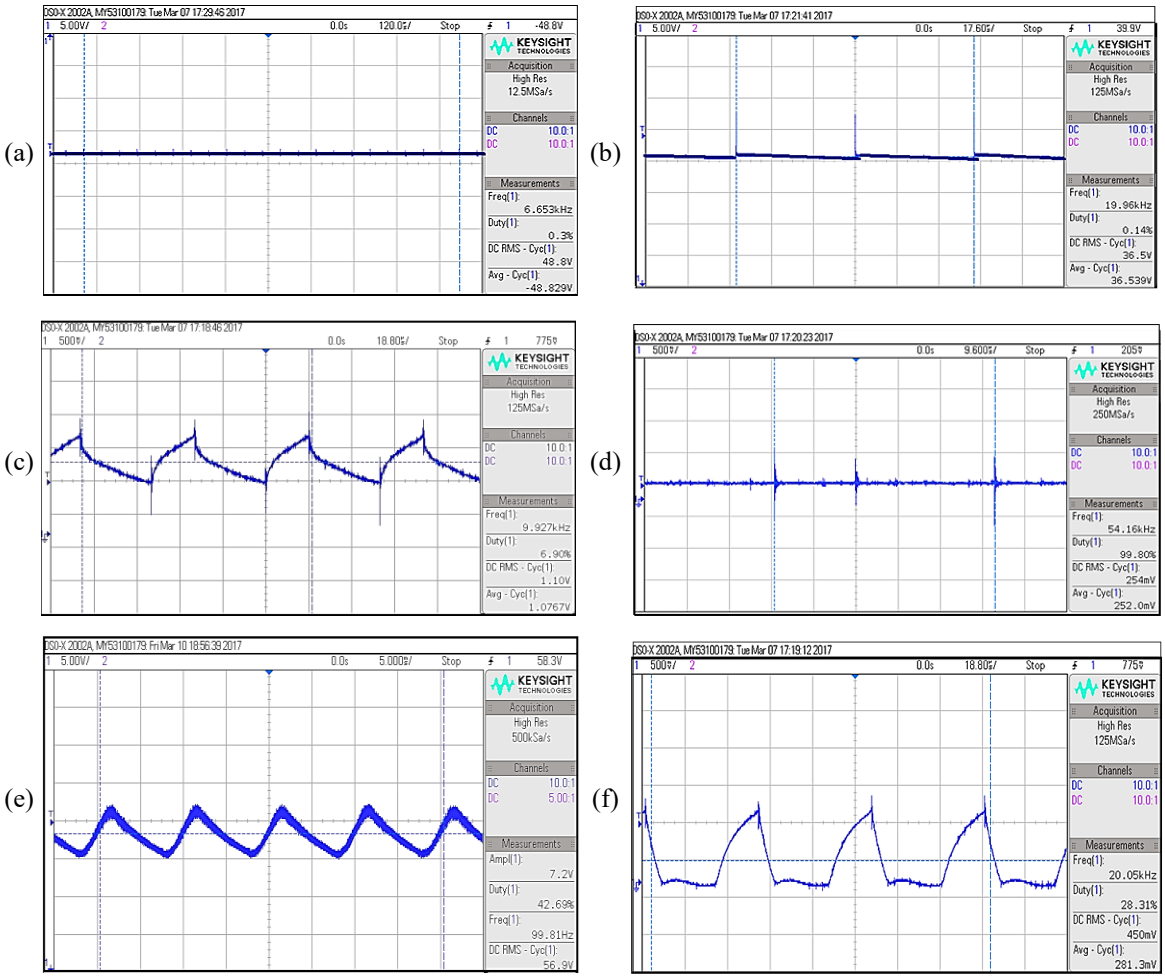

Figure17. Hardware results: (a) DC load voltage, (b) DC load current, (c) inductor VL_{3p}, (d) voltage across capacitor (C_o), (e) input voltage, and (f) input current

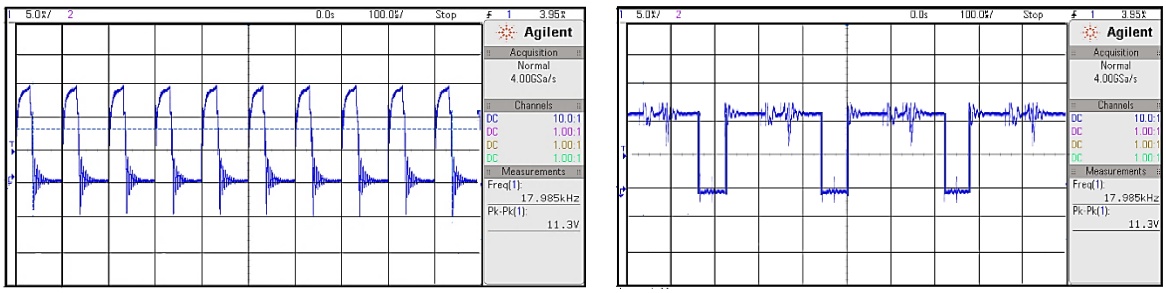

(a) (b)

Figure 18. Hardware results: (a) gate signals applied to Q_p and (b) gate signals applied to Q_n

5. CONCLUSION

Industries like automobile, textile, electronics technology, and construction suffer with some sustainable problems. Especially automobile industries need sustainable transportation solutions. This paper responds to the demand for sustainable practices by examining different control methods, including PWM, PID, back EMF, and spider controller algorithms. The speed of the BLDC motor is initially regulated using the PWM control technique. Following this, a PID controller is integrated with the BLDC motor, and system performance is evaluated by comparing the error to the reference signal. Additionally, other control methods like the back EMF observer and spider controller algorithm are employed for switching. All techniques are compared under no-load and fully loaded conditions of the BLDC motor. Simulation results indicate that the spider controller technique provides superior performance for BLDC motors. Based on the comprehensive comparison of various techniques, the spider switching controller technique emerges as the recommended choice for BLDC motors in EV applications. The results and discussions emphasize the advantages of using position sensors for speed control of BLDC motors, enhancing both reliability and efficiency. So, sensor control is the only way where higher performance is required. The proposed system controller is also implemented in hardware.

FUNDING INFORMATION

No funding involved.

AUTHOR CONTRIBUTIONS STATEMENT

This journal uses the Contributor Roles Taxonomy (CRediT) to recognize individual author contributions, reduce authorship disputes, and facilitate collaboration.

Name of Author	C	M	So	Va	Fo	I	R	D	O	E	Vi	Su	P	Fu
W. Margaret Amutha	✓	✓	✓	✓	✓	✓	✓	✓	✓	✓	✓	✓	✓	
S. Premalatha		✓		✓		✓		✓	✓	✓	✓	✓	✓	
M. Karthikeyan	✓		✓	✓	✓		✓			✓	✓		✓	

C : **C**onceptualization
M : **M**ethodology
So : **So**ftware
Va : **Va**lidation
Fo : **Fo**rmal analysis
I : **I**nvestigation
R : **R**esources
D : **D**ata Curation
O : Writing - **O**riginal Draft
E : Writing - Review & **E**diting
Vi : **Vi**sualization
Su : **Su**pervision
P : **P**roject administration
Fu : **Fu**nding acquisition

CONFLICT OF INTEREST STATEMENT

Authors state no conflict of interest.

DATA AVAILABILITY

Data availability is not applicable to this paper as no new data were created or analyzed in this study.

REFERENCES

[1] Y. Keda, S. Sameer, M. M. Khan, S. Shaikh, and S. Faisal, "Review on speed control techniques of brushless DC motor," 2019. [Online]. Available: https://api.semanticscholar.org/CorpusID:212548266.

[2] A. Dwivedi and A. N. Tiwari, "A review: speed control of Brushless DC motor," *IJBSTR Review Paper*, vol. 1, no. 6, pp. 14-19, Jun. 2013, doi: 10.13140/RG.2.2.10646.86087.

[3] S. Sakunthala, R. Kiranmayi, and P. N. Mandadi, "A study on industrial motor drives: comparison and applications of PMSM and BLDC motor drives," in *2017 International Conference on Energy, Communication, Data Analytics and Soft Computing (ICECDS)*, 2017, pp. 537-540, doi: 10.1109/ICECDS.2017.8390224.

[4] H. Wu, S. Cheng, and S. Cui, "A controller of brushless DC motor for electric vehicle," *IEEE Transactions on Magnetics*, vol. 41, no. 1, pp. 509-513, 2005, doi: 10.1109/ICEMS.2019.8922568.

[5] S. A. Kumar and S. A. E. Xavier, "Brushless DC motor speed control using microcontroller," *International Journal of Current Engineering and Scientific Research (IJCESR)*, ISSN (PRINT): 2393-8374, vol. 2, no.2, pp. 183-188, 2015, doi: 10.1109/iSSSC50941.2020.9358820.

[6] M. H. Zafar *et al*., "A novel meta-heuristic optimization algorithm based MPPT control technique for PV systems under complex partial shading condition," *Sustainable Energy Technologies and Assessments*, vol. 47, p. 101367, Oct. 2021, doi: 10.1016/j.seta.2021.101367.

[7] A. M. Ammar, F. M. Spliid, Y. Nour, and A. Knott, "Analysis and design of a charge-pump-based resonant AC–DC converter with inherent PFC capability," *IEEE Journal of Emerging and Selected Topics in Power Electronics*, vol. 8, no. 3, pp. 2067–2081, Sep. 2020, doi: 10.1109/JESTPE.2020.2966143.

[8] F. M. Spliid, A. M. Ammar, and A. Knott, "Analysis and design of a resonant power converter with a wide input voltage range for AC/DC applications," *IEEE Journal of Emerging and Selected Topics in Power Electronics,* vol. 8, no. 3, pp. 2056–2066, Sep. 2020, doi: 10.1109/JESTPE.2019.2963266.

[9] A. M. Ammar, F. M. Spliid, Y. Nour, and A. Knott, "A 1-MHz resonant led driver with charge-pump-based power factor correction," *IEEE Journal of Emerging and Selected Topics in Power Electronics*, vol. 9, no. 5, pp. 5838–5850, Oct. 2021, doi: 10.1109/JESTPE.2021.3083404.

[10] G. Li, J. Xia, K. Wang, Y. Deng, X. He, and Y. Wang, "A single-stage interleaved resonant bridgeless boost rectifier with high-frequency isolation," *IEEE Journal of Emerging and Selected Topics in Power Electronics*, vol. 8, no. 2, pp. 1767–1781, Jun. 2020, doi: 10.1109/JESTPE.2019.2912434.

[11] S. Sanjay and L. Raghavendra, "Adaptable speed bridgeless sepic converter VSI fed BLDC motor drive," in *2017 International Conference on Current Trends in Computer, Electrical, Electronics and Communication (CTCEEC)*, IEEE, Sep. 2017, pp. 1138–1143, doi: 10.1109/CTCEEC.2017.8455065.

[12] K. S. Devi, R. Dhanasekaran, and S. Muthulakshmi, "Improvement of speed control performance in BLDC motor using fuzzy PID controller," in *2016 International Conference on Advanced Communication Control and Computing Technologies (ICACCCT)*, IEEE, 2016, pp. 380-384, DOI: 10.1109/ICACCCT.2016.7831666.

[13] P. K. Singh, B. Singh, V. Bist, K. Al-Haddad, and A. Chandra, "BLDC motor drive based on bridgeless landsman PFC converter with single sensor and reduced stress on power devices," *IEEE Transactions on Industry Applications*, vol. 54, no. 1, pp. 625–635, 2018.

[14] J. Sriram and K. Sureshkumar, "Speed control of BLDC motor using fuzzy logic controller based on sensorless technique," in *2014 International Conference on Green Computing Communication and Electrical Engineering (ICGCCEE)*, IEEE, 2014, pp. 1-6, doi: 10.1109/ICGCCEE.2014.6922466.

[15] J. C. G. Real, E. Vázquez-Sánchez, and J. Gómez-Gil, "Position and speed control of brushless DC motors using sensorless techniques and application trends," *Sensors*, vol. 10, no. 7, pp. 6901-6947, 2010, DOI: 10.3390/s100706901.

[16] S. M. Awchar, S. P. Diwan, and P. Arlikar, "Advanced technique for speed control of sensorless BLDC motor," in *2018 Fourth International Conference on Computing Communication Control and Automation (ICCUBEA)*, IEEE, 2018, pp. 1–5, doi: 10.1109/ICCUBEA.2018.8697796.

[17] F. Rodriguez and A. Emadi, "A novel digital control technique for brushless DC motor drives," *IEEE Transactions on Industrial Electronics*, vol. 54, no. 5, pp. 2365-2373, 2007, doi: 10.1109/TIE.2007.900312.

[18] T. Shukla and S. Nikolovski, "A bridgeless Cuk-bb-converter-based BLDCM drive for MEV applications," *Energies*, vol. 16, no. 9, 2023, doi: 10.3390/en16093747.

[19] A. Rawat and M. F. Azeem, "Speed control of Brushless DC motor using modified genetic algorithm tuned fuzzy controller," *Current Journal of Applied Science and Technology*, vol. 39, no. 9, pp. 54–64, 2020, doi: 10.9734/cjast/2020/v39i930606.

[20] K. Murugesan and R. Ramasubbu, "Driving training-based optimization technique for estimating synchronous motor excitation current," *Bulletin of Electrical Engineering and Informatics*, vol. 14, no. 2, Apr. 2025, pp. 813–822, doi: 10.11591/eei.v14i2.8579.

[21] M. P. Sathe, S. Tetambe, S. Jadhav, and T. Khedekar, "Speed control of DC motor using PID controller-a review," *International Journal of Engineering Research and Technology*, vol. 6, no. 8, pp. 693–697, 2019, doi: 10.3923/ijert.2019.1212.1228.

[22] H. Jigang, F. Hui, and W. Jie, "A PI controller optimized with modified differential evolution algorithm for speed control of BLDC motor," *Automatika*, vol. 60, no. 2, pp. 135–148, 2019, doi: 10.1080/00051144.2019.1596014.

[23] S. P. Singh, K. K. Singh, K. S. Verma, J. Singh, and N. Tiwari, "A review on control of a brushless DC motor drive," *International Journal of Engineering Research and Technology*, vol. 9, no. 2, pp. 994–1002, 2019, doi: 10.3923/ijert.2019.1204.1098.

[24] B. Kumar, S. K. Swain, and N. Neogi, "Controller design for closed loop speed control of BLDC Motor," *International Journal on Electrical Engineering and Informatics*, vol. 9, no. 1, pp. 146, 2017, doi: 10.15676/ijeei.2017.9.1.10.

[25] M. Maharajan and S. A. E. Xavier, "Design of speed control and reduction of torque ripple factor in BLDC motor using spider-based controller," *IEEE Transactions on Power Electronics*, vol. 34, no. 8, pp. 7826–7837, 2018, doi: 10.1109/TPEL.2018.2880916.

[26] M. K. Merugumalla and P. K. Navuri, "Population algorithms for optimal control of BLDC motor drive," *HELIX*, vol. 8, no. 3, pp. 3350–3355, 2018, doi: 10.1016/helix.2018.03.064.

[27] A. Tashakori and M. Ektesabi, "Comparison of different PWM switching modes of BLDC motor as drive train of electric vehicles," *World Academy of Science, Engineering and Technology*, vol. 67, no.2, pp. 719–725, 2012.

[28] A. A. Obed and A. K. Kadhim, "Speed and current limiting control strategies for BLDC motor drive system: a comparative study*," International Journal of Advanced Engineering Research and Science*, vol. 5, no. 2, pp. 119–130, 2018.

[29] V. R. Walekar and S. V. Murkute, "Speed control of BLDC motor using PI & fuzzy approach: a comparative study," in *2018 International Conference on Information, Communication, Engineering and Technology (ICICET)*, IEEE, 2018, pp. 1–4, doi: 10.1109/ICICET.2018.8533778.

[30] D. Çelik and M. E. Meral, "A coordinated virtual impedance control scheme for three-phase four-leg inverters of electric vehicle to grid (V2G)," *Energy*, vol. 246, May 2022, doi: 10.1016/j.energy.2022.123354.
[31] M. E. Meral and D. Çelik, "Mitigation of DC-link voltage oscillations to reduce size of DC-side capacitor and improve lifetime of power converter," *Electric Power Systems Research*, vol. 194, Jan. 2021, doi: 10.1016/j.epsr.2021.107048.
[32] D. Çelik, "Lyapunov based harmonic compensation and charging with three-phase shunt active power filter in electrical vehicle applications," *International Journal of Electrical Power & Energy Systems,* vol. 136, 2022, doi: 10.1016/j.ijepes.2022.107564.
[33] T. Muthamizhan, P. Saravanan, and R. Maharana, "Sensorless control of Z-source inverter fed BLDC motor drive by FOC-DTC hybrid control strategy using fuzzy logic controller," in *2021 7th International Conference on Electrical Energy Systems, IEEE,* 2021, pp. 358–363, doi: 10.1109/ICEES51510.2021.9383752.
[34] L. Sun, "Low speed sensorless control method of Brushless DC motor based on pulse high frequency voltage injection," *Alexandria Engineering Journal*, vol. 61, no. 8, pp. 6457–6463, 2022, doi: 10.1109/AEJ.2015.2480760.
[35] A. Attar, J. Bouchnaif, and K. Grari, "Control of Brushless DC motors using sensorless Back-EMF integration method," *Materials Today: Proceedings*, vol. 45, pp. 7438–7443, 2021, doi: 10.1016/j.matpr.2021.01.861.

BIOGRAPHIES OF AUTHORS

W. Margaret Amutha is working as an assistant professor in Department of Electrical and Electronics Engineering, SRM Institute of Science and Technology, Ramapuram Campus, Chennai, India. She received her Ph.D. degree in SSN College of Engineering, Anna University, Chennai, B.E., M.E. degrees in Karunya Institute of Technology from Bharathiar University. She is currently working on hybrid energy storage systems for hybrid systems with the guidance of Dr. V. Rajini. She has published more than 20 papers in reputed journal. She can be contacted at email: margarew@srmist.edu.in.

S. Premalatha is an associate professor in Department of Electrical and Electronics Engineering, SRM Institute of Science and Technology, Ramapuram Campus, Chennai, India. She received her Ph.D. in Electrical Engineering from SRM University in 2015 and has 19 years of teaching experience. Her research interests include power quality, power converters, drives, renewable energy, FACTS, and electric vehicles. She can be contacted at email: premalas1@srmist.edu.in.

M. Karthikeyan received his B.E. Electrical and Electronics Engineering degree from Madurai Kamaraj University, M.E. Applied Electronics from Bharathiar University, and Ph.D. from Anna University, Chennai. He is an assistant professor at SRM Institute of Science and Technology, Ramapuram. His research interests include signal processing, machine learning, and deep learning applications to power system engineering. He can be contacted at email: karthikm14@srmist.edu.in.